Geochemistry Geophysics Geosystems G3
AN ELECTRONIC JOURNAL OF THE EARTH SCIENCES
Published by AGU and the Geochemical Society

Article
Volume 3, Number 10
10 October 2002
1055, doi:10.1029/2001GC000241
ISSN: 1525-2027

Physical interpretation of hysteresis loops: Micromagnetic modeling of fine particle magnetite

Lisa Tauxe
Scripps Institution of Oceanography, University of California, San Diego, La Jolla, California 92093-0220, USA (ltauxe@ucsd.edu)

H. Neal Bertram
Center for Magnetic Recording Research, 0401, University of California, San Diego, La Jolla, California 92093-0401, USA (nbertram@ucsd.edu)

Christian Seberino
Spawar Systems Center 2363, 53560 Hull Street, San Diego, California 92152-5001, USA (seberino@spawar.navy.mil)

[1] Hysteresis measurements have become an important part of characterizing magnetic behavior of rocks in paleomagnetic studies. Theoretical interpretation is often difficult owing to the complexity of mineral magnetism and published data sets demonstrate remanence and coercivity behavior that is currently unexplained. In the last decade, numerical micromagnetic modeling has been used to simulate magnetic particles. Such simulations reveal the existence of nonuniform remanent states between single and multidomain, known as the "flower" and "vortex" configurations. These suggest plausible explanations for many hysteresis measurements yet fall short of explaining high saturation remanence, high coercivity data such as those commonly observed in fine grained submarine basalts. In this paper, we review the theoretical and experimental progress to date in understanding hysteresis of geological materials. We extend numerical simulations to a greater variety of shapes and sizes, including random assemblages of particles and shapes more complex than simple rods and cubes. Our simulations provide plausible explanations for a wide range of hysteresis behavior.

Components: 11,218 words, 13 figures, 2 tables, 2 animations.

Keywords: Micromagnetic modeling; pseudo-single domain; hysteresis loops; rock magnetism.

Index Terms: 1540 Geomagnetism and Paleomagnetism: Rock and mineral magnetism; 1594 Geomagnetism and Paleomagnetism: Instruments and techniques; 1599 Geomagnetism and Paleomagnetism: General or miscellaneous.

Received 25 September 2001; **Revised** 4 February 2002; **Accepted** 10 April 2002; **Published** 10 October 2002.

Tauxe, L., H. N. Bertram, and C. Seberino, Physical interpretation of hysteresis loops: Micromagnetic modeling of fine particle magnetite, *Geochem. Geophys. Geosyst.*, *3*(10), 1055, doi:10.1029/2001GC000241, 2002.

1. Introduction

[2] Since the advent of readily available instruments capable of measuring hysteresis behavior of rock samples [e.g., *Flanders*, 1988], paleomagnetists have measured many different geological materials. Hysteresis is extremely sensitive to grain size, domain state, mineralogy, and state of stress. Virtually all geological materials of paleomagnetic interest have remanence and rever-

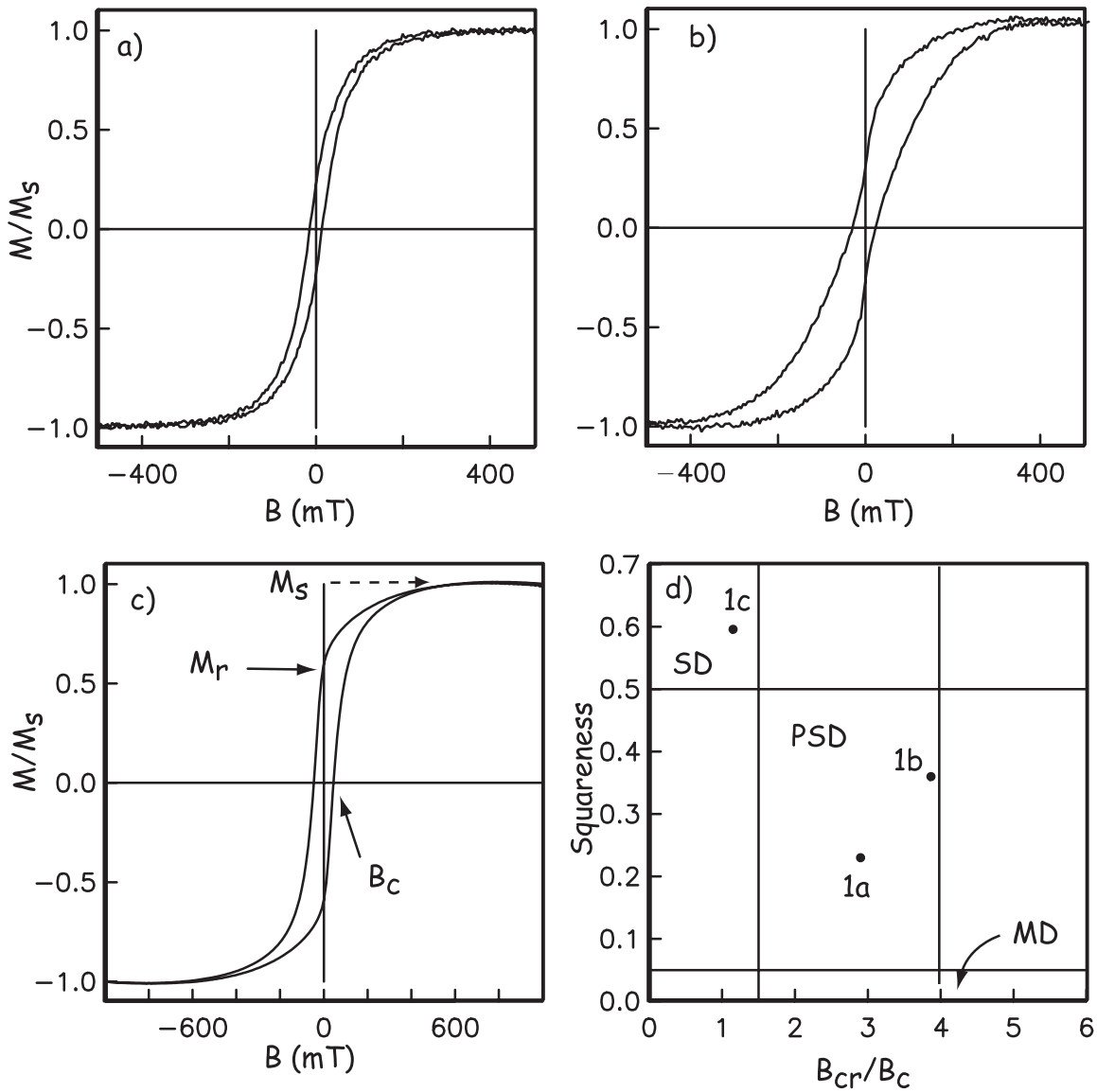

Figure 1. Representatives hysteresis loops from geological samples. (a) Typical "pseudosingle domain" hysteresis loop. (b) "Wasp-waisted" loop. (c) Hysteresis loop showing characteristic parameters, saturation remanence M_r, saturation magnetization M_s, and bulk coercive field B_c. (d) Plot of ratio of M_r/M_s (squareness) versus B_{cr}/B_c for samples shown in Figures 1a–1c. Boundaries of single-domain (SD), pseudosingle domain (PSD), and multidomain (MD) as drawn by *Day et al.* [1977].

sal properties dominated by nonuniform magnetization states. Magnetic modeling of hysteresis loops is therefore essential for understanding the origin of magnetic remanence and coercivity (see summary by *Dunlop and Özdemir* [1997]). The purpose of this paper is to present micromagnetic analyses that aid in understanding a variety of hysteresis behaviors. In addition, we review previous theoretical and experimental magnetic studies in the context of paleomagnetic research.

[3] The principal means in paleomagnetic research by which hysteresis loops such as those shown in Figures 1a–1c have been interpreted is through the use of the so-called "Day diagram" [*Day et al.*, 1977] (see Figure 1d). The Day diagram plots the saturation remanence M_r to saturation magnetization M_s ratio (here called "squareness") against the coercivity of remanence B_{cr} to coercive field B_c ratio (see Figure 1c for parameter definitions). (In this paper we will refer to the induction (with units

of tesla) using the term "field" sensu lato.) The term "squareness," common in the engineering literature, is useful because as squareness approaches unity, the hysteresis loop becomes more upright. B_{cr} (not shown) is the field required to reduce an initial saturation magnetic remanence to a demagnetized state. The remanence and coercivity ratios (dots in Figure 1d) earn the sample a designation of "single domain" (SD), pseudosingle domain "PSD" or "multidomain" (MD). Most samples used in paleomagnetic studies plot within the PSD field. The PSD designation in the environmental magnetism literature often leads to the conclusion that the sample has a magnetic mineralogy dominated by grains in the size range of 1–15 μm. This interpretation is based on the compilation by *Day et al.* [1977] of hysteresis parameters from crushed (titano)magnetites of known grain size. The grain size designations continue despite warnings of, for example, *Dunlop* [1986] and *Heider et al.* [1987] that the hysteresis behavior of crushed magnetic particles is quite different from uncrushed particles; hence the grain size assignments inferred from the Day diagram may not apply to many samples.

[4] In reality, the fact that hysteresis parameters lie within the "PSD" box on the Day diagram helps little in the interpretation of hysteresis loops in terms of grain size or domain state. For example, many loops (see, e.g., Figure 1b) have hysteresis parameters that plot within the PSD range, yet are distorted by mixing of SD and superparamagnetic (SP) grains [see, e.g., *Pick and Tauxe*, 1994; *Tauxe et al.*, 1996]).

[5] Data such as those shown in Figure 1c plot in the box labeled SD in the Day diagram (Figure 1d) and have been interpreted as being the result of magnetite dominated by cubic anisotropy [e.g., *Gee and Kent*, 1995]. This interpretation presents two difficulties. First, according to single domain theory, only equant grains of (titano)magnetite can have such high saturation remanences. Yet equant grains of (titano)magnetite have an extremely narrow (perhaps nonexistent) range for single domain behavior [e.g., *Butler and Banerjee*, 1975]. If the particle is too large, it divides itself into multiple domains (reducing saturation remanence), and if it is too small, the magnetization is dominated by thermal fluctuations; it is superparamagnetic and therefore contributes nothing to the remanence hence reduces the squareness [*Walker et al.*, 1993]). Second, hysteresis loops from cubic magnetite or TM60 should have coercive fields of the order of 10 mT [*Joffe and Heuberger*, 1974]. The loop shown in Figure 1c has a coercive field of ~45 mT, and many loops have coercive fields that are even higher (up to ~100 mT). In this paper, we present micromagnetic simulations that point the way to a plausible explanation for the high squareness and coercive field behavior illustrated in Figure 1c.

[6] The outline of this paper is as follows. In section 2 we briefly review analytical modeling of hysteresis of fine particles. In section 3 we discuss experimental results for which there are currently no clear explanations of the physical processes. An overview of numerical models is presented in section 4. The results of our numerical simulations are presented in section 5. Implications of these results are discussed in section 6, and our conclusions are summarized in section 7.

2. Analytical Modeling of Hysteresis

[7] The materials of interest here are ferrimagnetic. Micromagnetic modeling, whether analytic or numerical, attempts to determine the variation of magnetization vectors throughout a given sample. At every point, the material has a magnetization equal to the saturation magnetization. The distribution of magnetization orientations is found by minimizing the total magnetic energy. In general, the total magnetic energy density E_t of a magnetic particle can be expressed as

$$E_t = E_a + E_h + E_e + E_m + E_\sigma \quad (1)$$

where E_a is the magnetocrystalline anisotropy energy density and is minimized when the magnetization vectors are aligned in certain "easy" directions within the crystal. E_h is the energy arising from the torque on the magnetization vectors exerted by an external field. E_e is the exchange energy and is minimized when the magnetizations within the particle are aligned

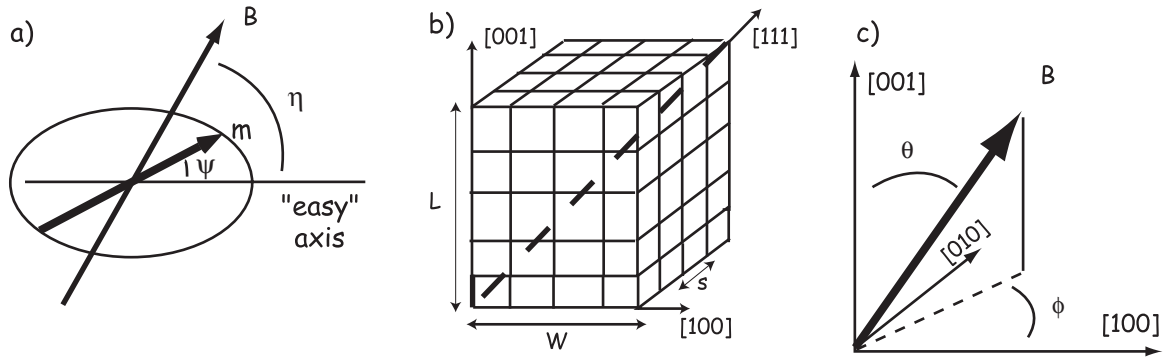

Figure 2. Frame of reference for micromagnetic modelling. (a) Relationship of applied field **B**, easy axis of magnetic particle and the magnetization vector **M** of the particle. η is the angle between the applied field and the easy axis, and ψ is the angle between the magnetization vector **M** and the easy axis. (b) Discretization scheme of the particle showing width *W*, length *L*, cell size *s* and the crystallographic axes [001], [100], [111]. Dimensions are quoted as W × W × L. (c) Relationship of the applied field to the crystallographic axes showing θ and ϕ.

parallel to one another. (Micromagnetic analysis is at a scale larger than atomic spacing; therefore ferrimagnetic materials are modelled by a positive exchange interaction.) E_m is the magnetostatic energy produced by the magnetic particle itself. When E_m is large enough this latter term can drive particles to seek a more demagnetized state resulting in complicated magnetization configurations. An example is the division of the magnetic particle into multiple regions of more or less uniform magnetization (magnetic domains). Finally, E_σ is the energy due to stress.

2.1. Uniformly Magnetized Particles

[8] For sufficiently small particles, the total magnetic energy is dominated by exchange. The magnetizations are essentially uniformly magnetized in the remanent state; this is called the single domain (SD) state. *Stoner and Wohlfarth* [1948] produced analytical solutions for single-domain noninteracting grains with uniaxial anisotropy in which the grains could be magnetized along one of two directions (parallel to the "easy axis"). In this case the energy density involves only the uniaxial anisotropy and the applied field:

$$E_t = K_u \sin^2\psi - M_s B \cos(\eta - \psi), \tag{2}$$

where η is the angle of the easy axis (shown as the long axis in Figure 2a) of the grain with respect to the applied field, *B*, and ψ is the angle of the magnetization vector with respect to the easy axis (see Figure 2a). For many materials of paleomagnetic interest, the uniaxial anisotropy arises from the shape of the magnetic particles and the anisotropy constant is given by

$$K_u = 1/2\mu_o(\Delta N)M_s^2, \tag{3}$$

where ΔN is a shape anisotropy factor that ranges from 0 for an equant particle to unity for a long needle.

[9] Another source of uniaxial anisotropy is stress (σ), which causes magnetic crystals to change shape and influences the magnetic energy. The fractional change in length dl/l is λ and the energy density related to stress is given by

$$E_\sigma = 3/2\lambda\sigma \cos^2\psi$$

where ψ is the angle between the magnetization vector and the principle stress axis. This is also a uniaxial anisotropy and can be incorporated into K_u if desired.

[10] The squareness *S* of a single particle is the projection of the saturation remanent magnetization onto the saturating field direction, hence for the uniaxial sindle domain case, $S = \cos\eta$ where η is as before (see Figure 2a). For an assemblage of particles, coercivity of remanence is the magnitude of the reverse field after saturation required to flip half the moments, resulting in zero net remanence. For a single particle, the coercivity of remanence is

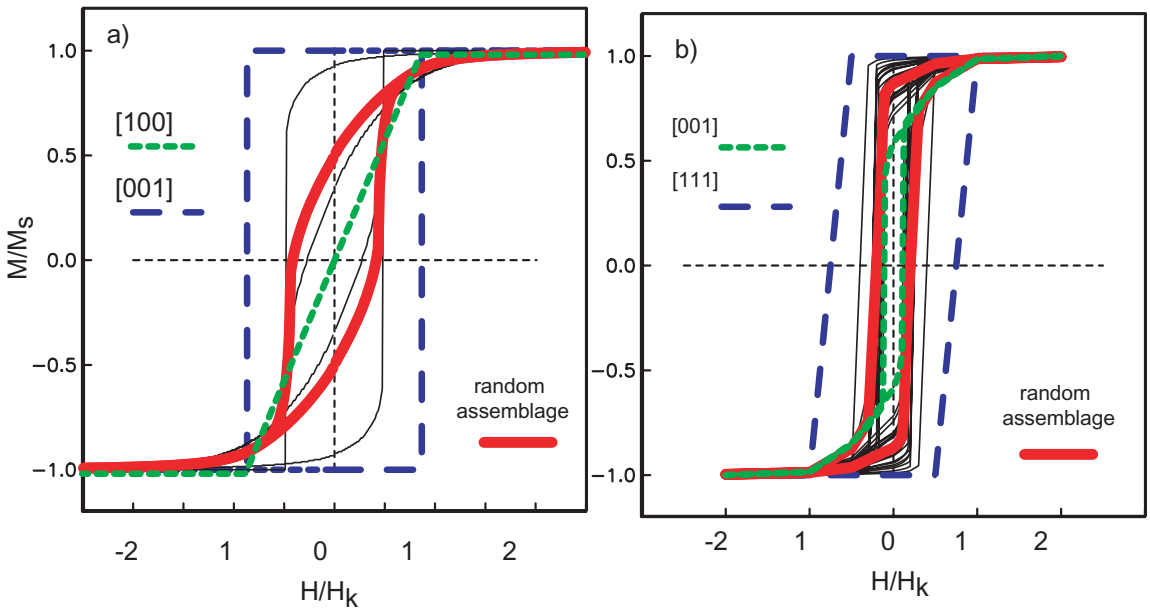

Figure 3. Heavy lines are theoretical behavior of 3-D random assemblages of (a) uniaxial and (b) equant grains of magnetite. Dashed lines are the responses along particular directions. Light grey lines are hysteresis response for single particles with various orientations with respect to the applied field.

the field required to flip the moment and is given by *Stoner and Wohlfarth* [1948] as

$$\frac{B_{cr}}{B_k} = \frac{(1 - t^2 + t^4)^{1/2}}{1 + t^2} = \frac{1}{\left(\cos^{1/3}\eta + \sin^{2/3}\eta\right)^{3/2}}, \quad (4)$$

where $t = \tan^{1/3}\eta$ and B_k is the intrinsic coercive field given by

$$B_k = 2K_u/M_s. \quad (5)$$

Coercivity of remanence differs from the coercive field in that the former is the field required to irreversibly flip the magnetization while the latter is the field required to reduce the net magnetization parallel to the applied field to zero. The former is always greater than or equal to the latter. As η goes from 0 to 90° the squareness goes from 1 to 0, and the ratio B_{cr}/B_c goes from 1 to infinity. For example, for a particle whose easy axis (taken as parallel to (001) in Figure 2b) is aligned with the applied field, $S = 1$ and $B_{cr}/B_c = 1$ (see outermost loop in Figure 3a). For $\eta = 90°$ (e.g., [100] as in Figure 2b), $S = 0$ and $B_{cr} = 0$, hence $B_{cr}/B_c = \infty$ (short dashed line in Figure 3a). The heavy curve in Figure 3a is for an assemblage of randomly oriented grains. Coercivity of remanence in this case is the field required to flip half the moments, reducing a saturation magnetization to zero. A random assemblage of uniaxial particles yields a loop with a squareness of 0.5, a ratio B_c/B_k of 0.48, and a ratio B_{cr}/B_c of 1.09 [*Wohlfarth*, 1958]. *Day et al.* [1977] used the $S = 0.5$ value to delimit the SD/PSD boundary but chose an arbitrary ratio of B_{cr}/B_c of 1.5 as the limit of single domain behavior (see Figure 1d).

[11] In the case of equant grains of magnetite, the anisotropy is controlled by crystal structure and has the cubic form

$$E_a = K_1\left(\alpha_1^2\alpha_2^2 + \alpha_2^2\alpha_3^2 + \alpha_3^2\alpha_1^2\right) + K_2\alpha_1^2\alpha_2^2\alpha_3^2, \quad (6)$$

where K_1 and K_2 are the constants of magnetocrystalline anisotropy and the αs are direction cosines between the magnetization vector **M** and the crystallographic axes [100, 010, 001]. In magnetite the magnetocrystalline anisotropy constant is negative, and the easy axis of magnetization is along one of four body diagonals (the [111] directions; see Figure 2b). TM60 has a positive K_1,

Table 1. Predictions for Randomly Oriented Assemblages of Particles Based on Classical Theory

K, J m^{-3}	M_s, A m^{-1}	S	B_k, mT	h	B_c, mT
$K_1 = -1.3 \times 10^4$	4.8×10^5	0.87	54	0.19	10
$K_1 = 2 \times 10^3$	1.2×10^5	0.83	34	0.32	11
$L/W = 1.3$; $K_u = 1.4 \times 10^4$	4.8×10^5	0.5	58	0.479	28
$L/W = 1.5$; $K_u = 1.4 \times 10^4$	4.8×10^5	0.5	85	0.479	41
$L/W = 2$; $K_u = 3.5 \times 10^4$	4.8×10^5	0.5	150	0.479	69
$L/W = \infty$; $K_u = 1.4 \times 10^5$	4.8×10^5	0.5	600	0.479	289

making the easy axis parallel to the cube edges. *Joffe and Heuberger* [1974] calculated squareness for a randomly oriented population of particles for $K_1 < 0$ to be 0.87 and B_c/B_k to be ~0.19 (see Figure 3b). For $K_1 > 0$, the loops are shorter and fatter with $S = 0.83$ and $B_c/B_k = 0.32$.

[12] For hysteresis to be dominated by uniaxial anisotropy, the particle dimensions must be such that $K_u > |K_1|$. For magnetite, we have $M_s = 4.8 \times 10^5$ Am^{-1} [*Smit and Wijn*, 1959]. The factor ΔN is readily determined [see, e.g., *Dunlop and Özdemir*, 1997]. For particles in which $L/W = 1.3$, $\Delta N = N_a - N_b = 0.1$. Using these numbers in equation (3), we have $K_u = 1.4 \times 10^4$ Jm^{-3}, which is slightly larger than $|K_1|$ for magnetite ($K_1 = -1.3 \times 10^4$ Jm^{-3} [*Joffe and Heuberger*, 1974]). Thus particles with only slight elongations should behave uniaxially (i.e., $S \leq 0.5$). Predicted coercive fields for other aspect ratios are shown in Table 1.

2.2. Nonuniform Reversal Mechanism

[13] The strength of the exchange energy determines the extent to which a particle can be nonuniformly magnetized. We can define a characteristic length, known as the exchange length l. Here we follow *Seberino* [2000] and define exchange length as

$$l = \sqrt{\frac{2A}{\mu_o M_s^2}}. \quad (7)$$

[14] For magnetite with $A = 1.33 \times 10^{-11}$ Jm^{-1} [*Heider and Williams*, 1988], so $l \sim 10$ nm.

[15] *Frei et al.* [1957] showed that for ellipsoidal particle shapes with diameters several times the exchange length, magnetization reversal can occur by a nonuniform "curling" mechanism. During reversal, the magnetization initially forms vortices about the axis, resulting in coercive fields that are lower than for the uniform reversal mechanism. The coercive fields of such particles decrease with increasing particle width. Small ellipsoidal particles are uniformly magnetized in the remanent state and do not reverse by curling, hence the squareness follows the Stoner–Wohlfarth model.

2.3. Superparamagnetism and Multidomain Particles

[16] Interpretation of hysteresis behavior requires that we also consider the critical sizes for superparamagnetic (SP) behavior and division into multiple domains (MD), both of which lower squareness. The SD/SP critical size depends on shape [*Butler and Banerjee*, 1975] varying from 30 to 50 nm, depending on the length to width ratio (more elongate particles having higher stability), although some investigators have estimated the SD/SP critical size as being somewhat smaller [see, e.g., *Tauxe et al.*, 1996]. The effect of the addition of superparamagnetic material to cubic SD (CSD) material on hysteresis loops was investigated theoretically (for $K_1 > 0$) by *Walker et al.* [1993] and numerically for uniaxial SD (USD) by *Tauxe et al.* [1996]. The SD/MD boundary is also strongly a function of shape [*Butler and Banerjee*, 1975]. For equant particles, it may in fact overlap the SD/SP boundary. In any case, there is at most an extremely narrow range of size and shape that will give values of squareness approaching the theoretical values for cubic anisotropy in (titano)magnetite.

2.4. Summary of Predictions From Analytical Models

[17] In Figure 4a and Table 1, we summarize the predictions for squareness and coercive field for

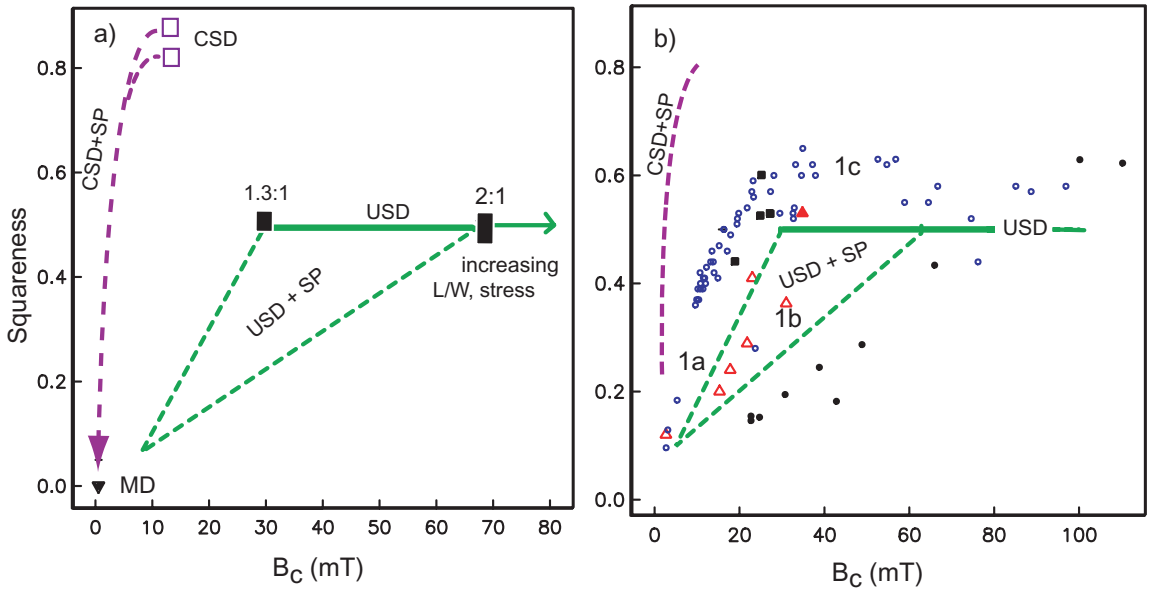

Figure 4. (a) Summary of theoretical predictions of squareness and coercive field B_c for randomly oriented populations of uniformly magnetized (titano)magnetite. Triangles labeled USD are predictions for uniaxial single domain magnetite with length to width ratios (L/W) of 1.3 and 2. CSD is the hypothetical cubic single domain. SP is superparamagnetic. Increasing L/W increases coercive field along the arrow. (b) Representative published data. Open triangles show data from *Dunlop* [1986], *Özdemir and Banerjee* [1982], *Levi and Merrill* [1978] on fine particle magnetite that has not been crushed. Solid triangle is for bacterial magnetite [*Moskowitz et al.*, 1988]. Small squares are data of *Schmidbauer and Schembera* [1987]. Small open circles show data from oceanic basalts [*Gee and Kent*, 1995]. Small filled dots indicate data from crushed magnetites [*Parry*, 1965]. Dashed lines are trends from Figure 4a for CSD plus SP and USD plus SP. Also shown are the data from the examples from Figure 1 (indicated by 1a, 1b, 1c respectively). The vast majority of data are unexplained by theory for uniformly magnetized particles.

randomly oriented particles of (titano)magnetite. The rectangles labeled 1.3:1 and 2:1 are the values predicted for uniaxial single-domain magnetite by *Stoner and Wohlfarth* [1948] for $L/W = 1.3$ and $L/W = 2$, respectively. As L/W increases, the coercive field will also increase to a maximum (when $\Delta N = 1$) of ~300 mT. The effect of stress on hysteresis parameters is to increase the uniaxial coercivity and behaves in the same manner as increasing the length to width ratio. The open squares labeled "CSD" are values for cubic single domain behavior for magnetite (upper) and TM60 (lower) predicted by *Joffe and Heuberger* [1974]. We plot these as open symbols because they are unlikely to be observed in room temperature measuremnts as this size and shape are predicted to be superparamagnetic by *Butler and Banerjee* [1975]. The values quoted by *Joffe and Heuberger* [1974] for $h \equiv B_c/B_k$ were converted to B_c using values for M_s and K_1 for magnetite and TM60 (see Table 1). The triangle labled "MD" is based on the multi-domain estimate of *Dunlop and Özdemir* [1997]. The effect of the addition of a superparamagnetic component to CSD was modelled by *Walker et al.* [1993]. Their estimates for squareness and coercive field (converted from h) are labeled "CSD + SP" in Figure 4a. *Tauxe et al.* [1996] investigated the effect of introducing superparamagnetic material to USD magnetite. Their simulations plot within the field labeled "USD + SP" in Figure 4a.

[18] We have replaced the traditional plot of squareness (referred to in the rock magnetic literature variously as M_r/M_s, M_{rs}/M_s, $sIRM/M_s$, J_r/J_s, etc.) versus B_{cr}/B_c or H_{cr}/H_c of *Day et al.* [1977] (e.g., Figure 1d) with a "squareness-coercive field" plot. We have done this partly because of the difficulty in estimating B_{cr} [see, e.g., *Fabian and von Dobeneck*, 1997] and partly because as shown by equation (4), it is poorly behaved for particles with large angles to the magnetic field. We have chosen instead to plot squareness versus bulk

coercive field. Coercive field is defined following the definition for "coercivity" sensu lato of *Stoner and Wohlfarth* [1948] as the field which brings the net magnetization parallel to the applied field to zero (see Figure 1c). Our squareness-coercive field plot is similar in some respects to the log–log plot of coercive field versus squareness of *Kent and Gee* [1996].

[19] Figure 4a delineates a number of regions with clear analytical explanations. There are also large areas with no explanation based on analytical theory. As we shall see in section 3, there are many published data sets that plot within these unexplained regions.

3. Experimental Data

[20] Analytical theory was challenged from the very beginning by the trends in coercivity of remanence and coercive field observed in size graded samples. Instead of showing an abrupt shift in coercive field at a particular grain size, the hypothetical MD/SD boundary, the data [e.g., *Gottschalk*, 1935; *Nagata*, 1953] showed a continuous change with grain size, suggesting a high degree of stability in grains that were theoretically too large to be uniformly magnetized.

[21] The origin of the SD-like behavior in large magnetic grains has thus been the subject of debate through out the history of rock magnetism (see *Dunlop and Özdemir* [1997] for a useful summary). *Verhoogen* [1959] envisioned a single domain core stabilized by dislocations nestled within large multidomain grains, a notion amplified by *Shive* [1969] and *Fabian and Hubert* [1999]. *Stacey* [1961] was the first to call the transitional behavior "pseudo-single domain" and suggested that irregular shapes caused unequal domain sizes which would give rise to a net moment [see, also, *Stacey*, 1962, 1963]. *Stacey and Banerjee* [1974] noted that small grains with a single wall could have a considerable net moment due to the wall itself. However, *Dunlop* [1973] suggested that none of these ideas could satisfy theoretical or experimental results and invoked particles with "wavelike" spin structures as the cause of PSD behavior. He drew on the curling mode of moment reversal [*Frei et al.*, 1957] as an analogy, viewing this curling style of remanence as a type of "wall."

[22] *Halgedahl and Fuller* [1983] documented "too few" domain walls in large titanomagnetite grains using a technique of imaging domain walls on smooth surfaces with ferric colloids. The failure to nucleate domain walls was interpreted as the source of PSD behavior. While this may be the case for large grains with high stability, it is also true that there may be other significant causes of PSD behavior, particularly in small grains.

[23] Through careful examination of hysteresis parameters as a function of grain size, *Dunlop* [1986] demonstrated that there are in fact two trends of coercive field versus grain size, one for grains prepared by crushing [e.g., *Parry et al.*, 1965] and one for grains prepared without crushing. Squareness-coercive field relationships for the two types of grains are shown in Figure 4b. Large (1–15 μm) crushed grains (black dots) display comparable squareness but much higher coercive fields than small uncrushed grains (open triangles). Coincidentally, when plotted on the Day diagram, these two data sets overlay one another.

[24] Grains as large as 1–15 μm theoretically should have domain walls and have vanishingly small squareness and coercive fields. The unexpected stability of the large crushed grains is thought to be caused by the role of stress which acts to increase the uniaxial magnetic anisotropy constant, hence B_c [see, also, *Heider et al.*, 1987].

[25] *Schmidbauer and Schembera* [1987] measured carefully sized magnetites at 130°K, just above the temperature at which K_1 changes sign. They found a third trend in squareness and coercive field with puzzling maxima in both at ~80 nm (see Table 2). They hypothesized that the difference between their data and the room temperature data was caused by the complicating addition of superparamagnetic fractions in the room temperature data (SP behavior is suppressed at low temperature). They also proposed that the maxima in squareness and coercive field were caused by more complex spin structures.

[26] Indeed, the room temperature (uncrushed) data (open triangles in Figure 4b) plot exactly in the

Table 2. Hysteresis Parameters From Sized Magnetites, 130 K[a]

W, nm	σ	S	B_c, mT
61	25	0.525	25
85	25	0.6	25.3
127	35	0.44	19
162	45	0.19	16

[a] W is mean width, σ is the standard deviation, S is squareness, and B_c is the coercive field.

region predicted for USD magnetite plus a superparamagnetic fraction, except the data from magnetotactic bacteria (shown as the solid triangle) of *Moskowitz* [1988]. These have squarenesses in excess of 0.5 as do most of the low temperature data of *Schmidbauer and Schembera* [1987]. The lack of an apparent SP component in the magnetotactic bacteria is consistent with the tighter grain size control allowed by the biotic processes; these presumably tune crystal growth to maximize squareness and minimize the effect of superparamagnetism (see *Dunin-Borkowski et al.* [1998] for a description of sizes and shapes of magnetites from the species measured by *Moskowitz* [1988]).

[27] Also shown in Figure 4b are the data from oceanic basalts [*Gee and Kent*, 1995] (small open circles). These show a puzzling trend of high values for both squareness and coercive field. They do not appear to be consistent with a mixture of cubic anisotropy and superparamagnetic behavior, having much higher coercive fields than the trend for CSD plus SP from Figure 4a. Nor are they likely to be a mixture of USD plus CSD which would presumably plot along a CSD-USD mixing curve. Instead, these data plot orthogonal to such a hypothetical mixing trend. Moreover, while magnetostriction (stress) will act to increase the coercive field, it can do nothing to enhance squareness, being an essentially uniaxial phenomenon. In fact, it is difficult to explain these data with any analytical model so far considered; they plot in an unexplained region with squareness values higher than those allowed by uniaxial models and coercive fields much higher than those allowed by cubic models of anisotropy.

[28] We have now reached the limit of what analytical theory can predict and find the answers lacking for a number of different data sets that plot in unexplained regions of the squareness-coercive field diagram. The key to understanding these unexplained data must lie in the details of the internal magnetization states, which are by nature extremely complicated and inaccessible to analytical theory. We require therefore numerical models in which investigations are possible of nonuniform magnetic states.

4. Numerical Models of Hysteresis

[29] In section 3, we reviewed basically analytical approaches for the understanding of magnetic behavior. Such solutions are only useful for simple cases, such as uniformly magnetized particles. Nonuniform magnetization states within crystals must be determined by micromagnetic techniques [e.g., *Brown*, 1963] requiring numerical simulations on fast computers.

[30] Realistic 3-D micromagnetic models first appeared in the late 1980s [*Schabes and Bertram*, 1988; *Williams and Dunlop*, 1989]. These simulations showed a prevalence of magnetic remanent states that were neither uniformly magnetized (as in a strict single domain particle) nor multidomain with true domain walls. *Schabes and Bertram* [1988] described "flower" and "vortex" remanent states in cubic particles with uniaxial anisotropy as illustrated in Figures 5a and 5b, respectively. In the flower remanent state, the magnetizations spread outward toward the cube corners and are essentially uniformly magnetized in the center of the grain. In the vortex remanent state, the magnetizations rotate around the cube centers. Generally speaking, the vortices are prevalent at the tips of the particles. Note that nonuniform equilibrium states occur wherever partical shapes are nonellipsoidal, but the smaller the particle, the more uniform the magnetization.

[31] The simulated particles of *Schabes and Bertram* [1988] evolved from an essentially uniformly magnetized (SD) remanent state through the flower state to the vortex state as the particle width increased. Particles in the nonuniform remanent states are not at saturation, hence exhibit lower values of squareness than true SD grains. *Schabes*

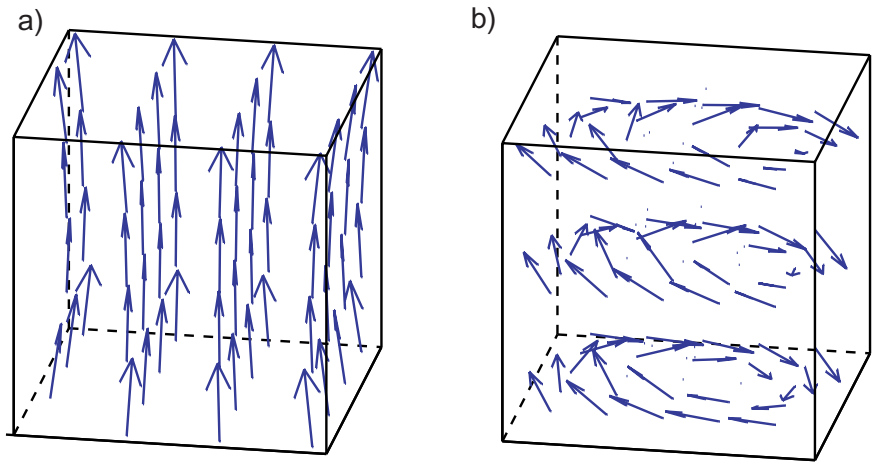

Figure 5. (a) "Flower" remanent state and (b) "vortex" remanent state as described by *Schabes and Bertram* [1988].

and Bertram [1988] also showed that, in contrast to squareness, the coercive field did not decrease continuously with particle width. For sizes that exhibited a pronounced flower state, the coercive fields were larger than those of smaller SD grains. When the width increased to the point at which the vortex remanent state emerged, the magnetization reversed by a curling type mode, which led to a strong decrease in coercive field.

[32] Since these early 3-D models, there has been much progress in modeling of magnetic materials using parameters of interest to rock magnetists [see, e.g., *Williams and Dunlop*, 1995; *Fabian et al.*, 1996; *Williams and Wright*, 1998; *Rave et al.*, 1998; *Muxworthy and Williams*, 1999a, 1999b; *Newell and Merrill*, 2000a, 2000b]. In this paper, we build on the previous work, hence a brief review is in order. *Williams and Dunlop* [1995] simulated magnetic hysteresis in magnetite cubes and parallelopipeds (aspect ratio of 1.7:1) with the external field aligned along the "easy" and "hard" axes for the size range 0.1–0.7 μm. They found decreasing coercive field and squareness with increasing grain size. They further suggested that grains whose remanent state is a vortex are responsible for PSD behavior. *Fabian et al.* [1996] investigated the remanent states of magnetite grains with aspect ratios ranging from 1:1 to 2.74:1 and sizes from 0.05 to 0.6 μm. They determined approximate threshold sizes for SD-PSD behavior by estimating the energies of the flower and vortex remanent states as a function of grain size. PSD values of squareness become evident when the vortex remanent state is favored.

[33] *Muxworthy and Williams* [1999a, 1999b] incorporated temperature into their simulations. They investigated the behavior of magnetite near the Verwey transition and as a function of temperature. *Newell and Merrill* [2000a] investigated the change from the flower remanent state to the vortex remanent state in simulations of cubes whose magnetic anisotropy were uniaxial. They warned of the instability of the numerical simulations and suggested several strategies for avoiding unstable solutions. In a companion paper, *Newell and Merrill* [2000b] simulated the hysteresis behavior of cubes and cuboids (neglecting the effect of magnetocrystalline anisotropy) in order to investigate the Day diagram, pointing out many difficulties with grain size predictions.

[34] In the following, we will present our numerical simulations of magnetic particles in the range of 20 to 140 nm (0.02 to 0.14 μm) with various aspect ratios. Our simulations take into account magnetocrystalline anisotropy and attempt to characterize the effects of size, shape, and orientation with the external field. We are particularly interested in finding plausible explanations for hysteresis behavior observed in paleomagnetic studies for which there is currently no understanding, in particular, grains that have coercive fields higher than allowed

for cubic anisotropy and squarenesses higher than allowed by uniaxial anisotropy in magnetite.

[35] One technique in numerical micromagnetics is to discretize particles into cubic elements in which each cell has a uniform magnetization (see *Bertram and Zhu* [1992] and Figure 2b). (Finite element techniques are also commonly used; see *Yang and Fredkin* [1996].) The cell dimension is here called s. Each cell has a total energy following equation (1). The exchange energy E_e arises from coupling to neighboring cells, while the magnetostatic energy E_m involves interaction with all the other cells. It is the magnetostatic energy that makes numerical micromagnetics so computer intensive.

[36] Equilibrium configurations of magnetization vectors $\mathbf{M}$ within the cells are found by minimizing the torque $\mathbf{M} \times \mathbf{B}_{\text{eff}}$ or equivalently, aligning the magnetization $\mathbf{M}$ along the effective field $\mathbf{B}_{\text{eff}} = -\partial E/\partial \mathbf{M}$. Because the effective field depends on the magnetizations of all the other cells, an iterative process is generally used. Magnetization processes are generally dynamic so that given an initial configuration (e.g., saturation), the system evolves to minimum energy following:

$$\frac{dE}{dt} = -\left(\frac{\alpha_d \gamma_e}{M_s}\right)|\mathbf{M} \times \mathbf{B}_{\text{eff}}|^2 \tag{8}$$

where t denotes time, γ_e denotes the gyromagnetic ratio of the electron (1.76×10^{11} T$^{-1}s^{-1}$) and α_d is a dimensionless damping parameter. Using equation (1) and assuming uniaxial anisotropy, $\mathbf{B}_{\text{eff}}$ is given by:

$$\mathbf{B}_{\text{eff}} = \mathbf{B}_o + \mathbf{B}_m + \left(\frac{2K_u}{M_s}\right)\left(\frac{\mathbf{M}\cdot\hat{k}}{M_s}\right)\hat{k} + \left(\frac{2A}{M_s}\right)\left(\frac{\nabla^2\mathbf{M}}{M_s}\right) \tag{9}$$

where $\mathbf{B}_o$ is the external field, $\mathbf{B}_m$ is the magnetostatic interaction field, $\hat{k}$ is parallel to the easy axis (the axis of elongation), A is the exchange constant as in equation (7), and M_s is the saturation magnetization. For systems with cubic anisotropy, the anisotropy term in equation (9) is replaced by a suitable derivitive of equation (6). In the case of magnetite at room temperature, the easy axis is parallel to the (111) direction as shown in Figure 2b.

[37] Magnetization relaxation typically occurs on the order of a nanosecond so that in our studies, hysteresis processes are quasi-static. To find the magnetization equilibrium along each point in a hysteresis loop, two methods are typically used. The first realigns, at each step, the magnetization in each cell iteratively along the effective field to minimize the energy [*Rave et al.*, 1998]. We use a different technique here. We simply integrate the coupled Landau–Lifshitz equation [see *Bertram and Zhu*, 1992]:

$$\frac{d\mathbf{M}}{dt} = -\gamma_e \mathbf{M} \times \mathbf{B}_{\text{eff}} - \left(\frac{\alpha_d \gamma_e}{M_s}\right)\mathbf{M} \times (\mathbf{M} \times \mathbf{B}_{\text{eff}}). \tag{10}$$

Because we are not specifically interested in dynamics, we adjust α_d for a rapid numerical solution.

[38] In order to design discretization schemes sufficiently detailed to represent accurately the magnetization state, we consider the length l (defined in equation (7)) over which exchange energy dominates and magnetization vectors are essentially parallel. We have found that for our simulations, s should be no more than twice l, so the number of cells must increase as the particle width W grows. To ensure stability of our results, we have also verified all results near the $2l$ limit with multiple discretization schemes.

[39] Equation (10) is a "stiff" differential equation. This means that the usual numerical techniques have poor stability except for very small time steps. We use the LSODES stiff solver developed by Alan C. Hindmarsh of Lawrence Livermore National Laboratory.

[40] For the computations presented here, we have in all cases started with the magnetizations set parallel to the magnetic field direction, then applied a saturation magnetic field equal to $\mu_o M_s$. (For the case of magnetite, this is ~0.6 T.) We then decrease the field in small increments to zero and evaluate the squareness. The sign of $\mathbf{B}$ is is then reversed and increased in small increments until the magnetization parallel to the applied field direction is zero ($\equiv B_c$). Some simulations were carried out to $-\mu_o M_s$.

[41] In order to achieve the computations necessary in a reasonable amount of time, we use a Fast Multipole Method (FMM) [see *Seberino and Bertram*, 2001]. This method reduces the computational cost of calculating the magnetostatic field and scales asymptotically linearly with the problem size. All calculations were done using a four node Beowulf parallel processing system (MrBrown in the Center for Magnetic Recording Research at University of California, San Diego).

[42] As noted earlier, we neglect magnetostriction. It is worth reiterating, however, that inclusion of magnetostriction in the modeling will not help explain the high squareness behavior. As magnetostriction behaves uniaxially, it faces the same upper limit of 0.5 that shape induced anisotropy has. We also neglect thermal fluctuations in our model; they are beyond the scope of the present investigation. The parameters that we do take into account are particle size, shape, first-order magnetocrystalline anisotropy, exchange, and saturation magnetization. All simulations were done assuming the parameters for magnetite already mentioned in the preceding text. In this work, we have studied the magnetization structure, squareness, and coercive field as a function of particle width, length, and shape and orientation with respect to the applied field.

5. Simulation Results

[43] We present our results in order of increasing complexity, starting with those for magnetite cubes of various sizes and discretization schemes in section 5.1. We consider the effect of elongation for essentially uniformly magnetized particles in section 5.2. This is done by increasing aspect ratios from 1:1 to 2:1, keeping particle width constant. We then consider the effect of size on particles with a 2:1 aspect ratio in section 5.3. More complex shapes are considered in section 5.4. Finally, in section 5.5, we present results from simulations of uniformly oriented arrays of particles.

5.1. Magnetite Cubes

[44] We begin by examining the state of magnetization in cubes that have been saturated with a field parallel to the (001) axis (see Figure 2b) and allowed to relax into a zero field as described in the previous section. We vary grain size from 20 to 140 nm and discretization schemes ranging from $4 \times 4 \times 4$ to $7 \times 7 \times 7$. Note that in these simulations, the easy axis of magnetization is along the body diagonal (111) as dictated by the magnetocrystalline anisotropy term.

[45] When the grain width is small (W in the range of 20–60 nm), the moments align essentially parallel to the body diagonal as shown in Figure 6a. As the width increases, the magnetization becomes increasingly complex. Figure 6b shows the remanent state for $W = 70$ nm from a $5 \times 5 \times 5$ simulation. This is a "flower" type remanent state. A typical vortex remanent state is achieved with $W = 115$ nm as shown in Figure 6c. (For clarity we show only odd numbered layers.) Finally, with $W =$ 140 nm (Figure 6d), the remanence state is multidomain, exhibiting approximately two domains.

[46] The net remanence parallel to the applied field as a fraction of saturation (squareness) of the grain shown in Figure 6a and 6b is 0.57. The squareness for the grain shown in Figure 6c is 0.18 and Figure 6d is 0.02. We plot squareness versus width in Figure 7a for the particles shown in Figure 6 as well as other simulations at intermediate particle sizes. Squareness values are relatively constant, equal to the single domain value for $W < 70$ nm, but decrease thereafter as substantial nonuniform remanent states occur. At the largest size ($W = 140$ nm), the particle is essentially demagnetized in the remanent state.

[47] We plot the simulated coercive field versus width in Figure 7b. The theoretical single domain value of coercive field for fields applied parallel to (001) is $\sim 0.112 B_k$ or $\sim$6 mT. The simulated values for coercive field versus grain size are very close to the expectation value for $W < 60$ nm. For $W > 60$, there is a considerable increase in coercive field, corresponding to the flower state (Figure 6b). The peak in coercive field prior to development of the vortex structure is reminiscent of that seen by *Schabes and Bertram* [1988]. With a further increase in particle width, coercive field decreases steadily, associated with the onset of the vortex

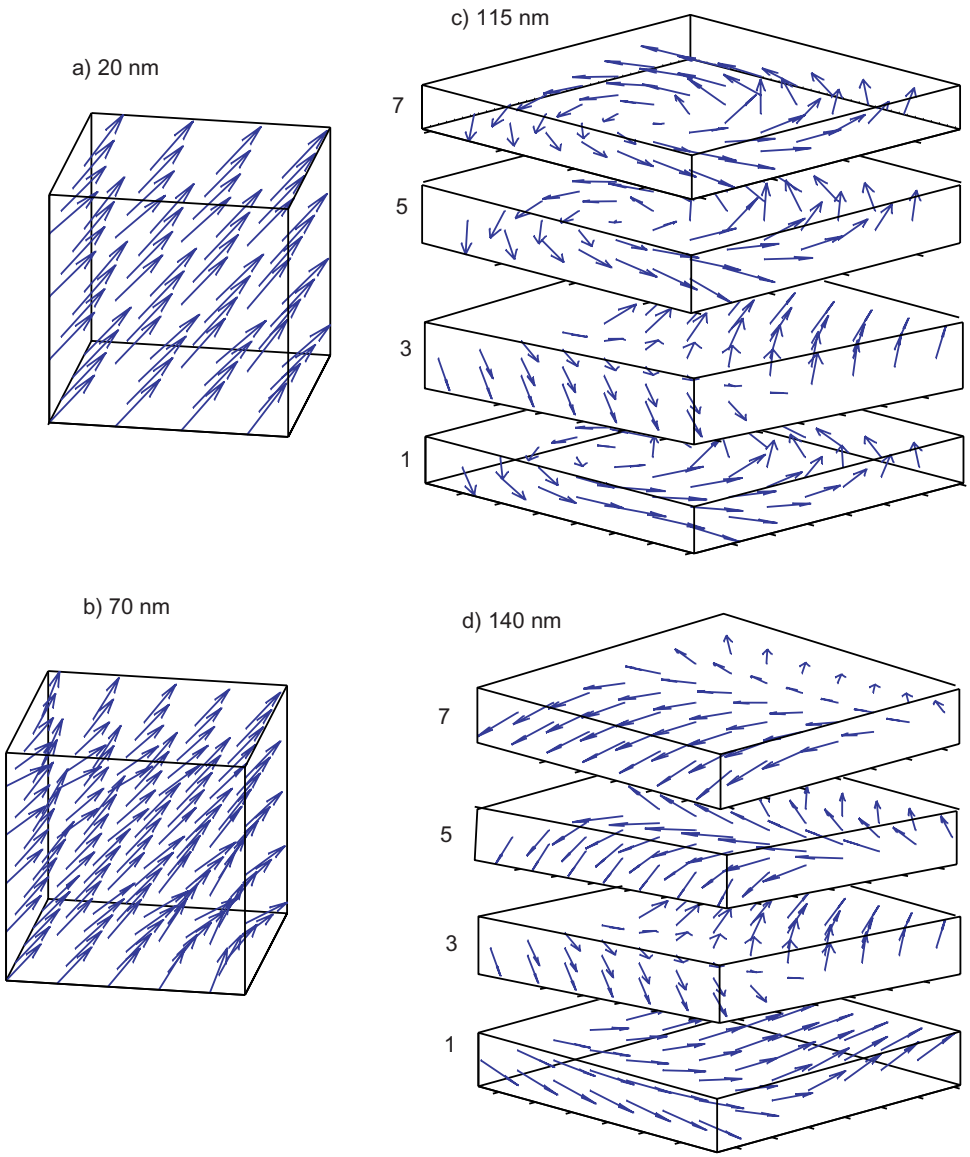

Figure 6. Magnetic vectors of cells from selected simulations. (a) A 4 × 4 × 4 simulation of a 20 nm grain. The grain is magnetized along the body diagonal as expected from SD magnetite. (b) A 5 × 5 × 5 simulation of a 70 nm grain. The magnetic vectors are in a "flower" state. (c) A 7 × 7 × 7 simulation of a 115 nm grain. Only odd numbered layers are shown for clarity. This grain is in a vortex state, giving a lower net moment along the field direction. (d) A 7 × 7 × 7 simulation of a 140 nm grain. Plotted as in Figure 6c. This grain has two domains and has a very low net magnetization and coercive field.

remanent state (see Figure 6c), until typical multidomain values are achieved by W = 140 nm.

[48] Animations 1 and 2 show the reversal process during a simulated hysteresis experiment for 60 nm (flower remanent state) and 115 nm (vortex remanent state) particles (animations are found in the HTML version of this article at http://www.g-cubed.org). Note the strikingly different styles of reversal whereby the smaller particle reverses nearly more or less coherently while the larger particle undergoes reversal by curling.

5.2. Transition From Cubic to Uniaxial

[49] As discussed earlier, analytical theory predicts that shape anisotropy will dominate over magnetocrystalline anisotropy at elongation values (L/W) exceeding ~1.3 (see Table 1). Below that, single

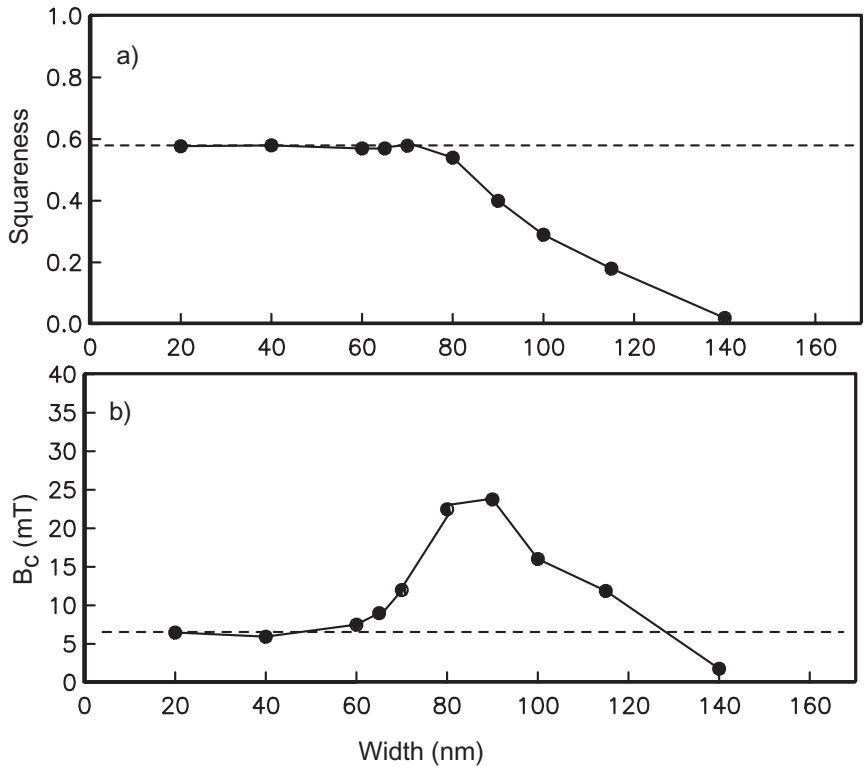

Figure 7. (a) Net magnetization parallel to applied field direction (squareness) as a function of grain width W. The expected value for SD magnetite is 0.57 (cubic anisotropy). (b) Coercive field (B_c) versus width for simulations. The expected value for SD magnetite is 6 mT.

domain particles are expected to have their remanent magnetizations aligned with the [111] direction closest to the direction along which the saturating field was applied. Above that aspect ratio, they are expected to have moments aligned along the long axis in the direction with the least angle to the last applied (saturating) field. Thus squareness for a magnetocrystalline dominated particle would be 0.57 for fields applied parallel to [001] and [010] and 1.0 for fields applied parallel to [111]. For uniaxial particles, squareness should be 1.0 for fields applied parallel to the elongation axis and zero for fields applied perpendicular to it. Note that for these simulations, we have elongated the particles parallel to the [001] crystallographic axis. This may not be the case in "real" particles, but it serves the purpose of examining the separate contributions of magnetocrystalline and shape anisotropy to hysteresis behavior.

[50] We plot the results of our simulations as a function of aspect ratio L/W and direction of the applied field in Figure 8a and Figure 8b. The particle width for all these simulations was W = 20 nm; the magnetization remanence and coercive field were therefore those of uniformly magnetized particles. These results show a more complicated behavior than that predicted for strictly cubic or uniaxial behavior. There is a broad transition from magnetocrystalline behavior for equant grains to uniaxial behavior at $L/W \sim 1.5$. Particles in the transition zone ($1 < L/W < 1.5$) have remanent magnetizations aligned with the long axis (here called [001]) if the field was applied parallel to it and aligned at an angle between the [111] and the long axis when the field was applied either parallel to [111] or [010] (the short axis).

[51] On the basis of these results, we anticipate that randomly oriented assemblages of slightly elongate particles will have hysteresis behavior intermediate between uniaxial and cubic particles. They will have higher squareness and lower coercive fields than the uniaxial case and lower

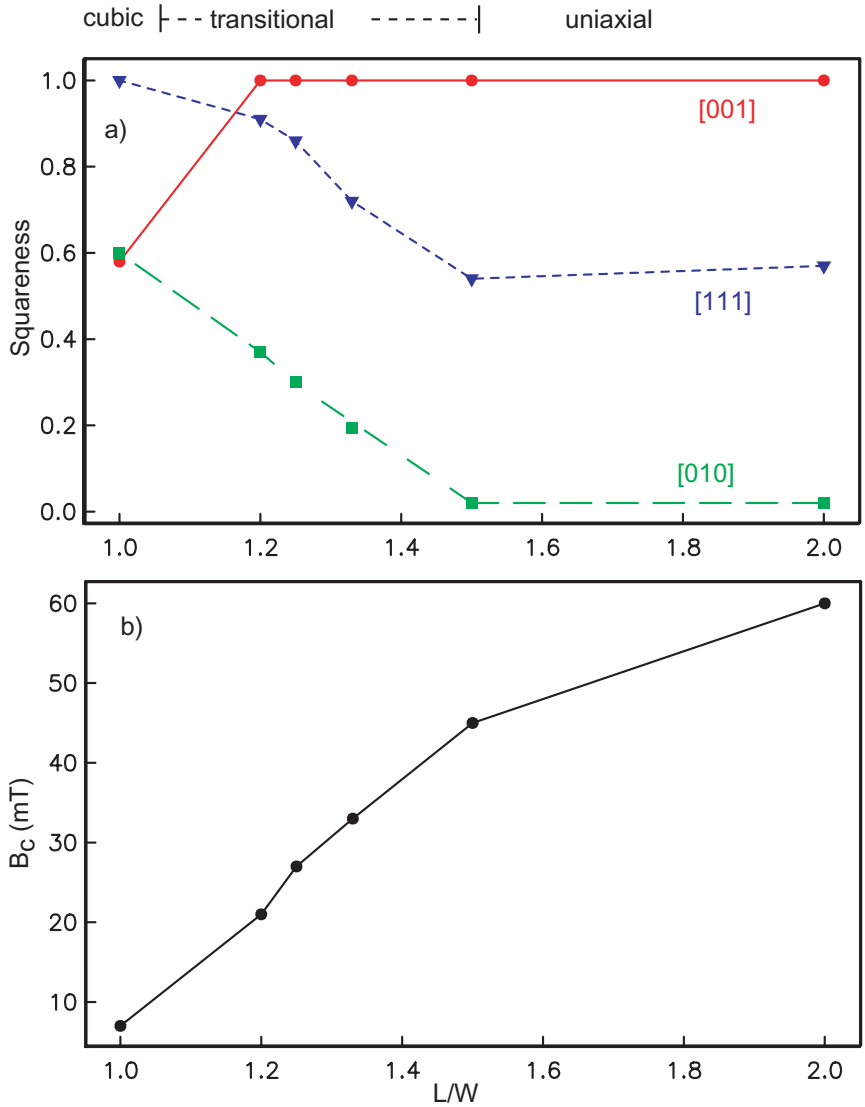

Figure 8. (a) Values for squareness from simulations of a 20 nm particle versus length to width ratio (L/W). The three lines are for the different angles of the applied field: dots are for applied field parallel to the long axis [labelled 001], triangles are for applied field parallel to the magnetocrystalline axis [111] and squares are for the field applied perpendicular to the long axis [labeled 010]. (b) Coercive field (B_c) plotted against aspect ratio (L/W). See Table 1 for expectation values for various L/W.

squareness but higher coercive fields than the cubic case.

5.3. Uniaxial Anisotropy

[52] Here we consider particles that are dominated by shape anisotropy ($L/W \geq 2$). In these examples, the field is applied parallel to the long axis. In Figure 9 we show remanence states from simulations after exposure to saturating fields parallel to the particle length. We show representative results ranging in size from $W = 40$ nm to $W = 120$ nm for particles with length to width ratios fixed at $L/W = 2$. From the results of the previous section, we expect these particles to exhibit uniaxial behavior. The smallest particle (shown in Figure 9a) is 40 nm and is in a flower state with the magnetization very nearly at saturation. As the particle size increases, the degree of "flowering" increases as illustrated by the simulation for the 70 nm particle in Figure 9b. Above

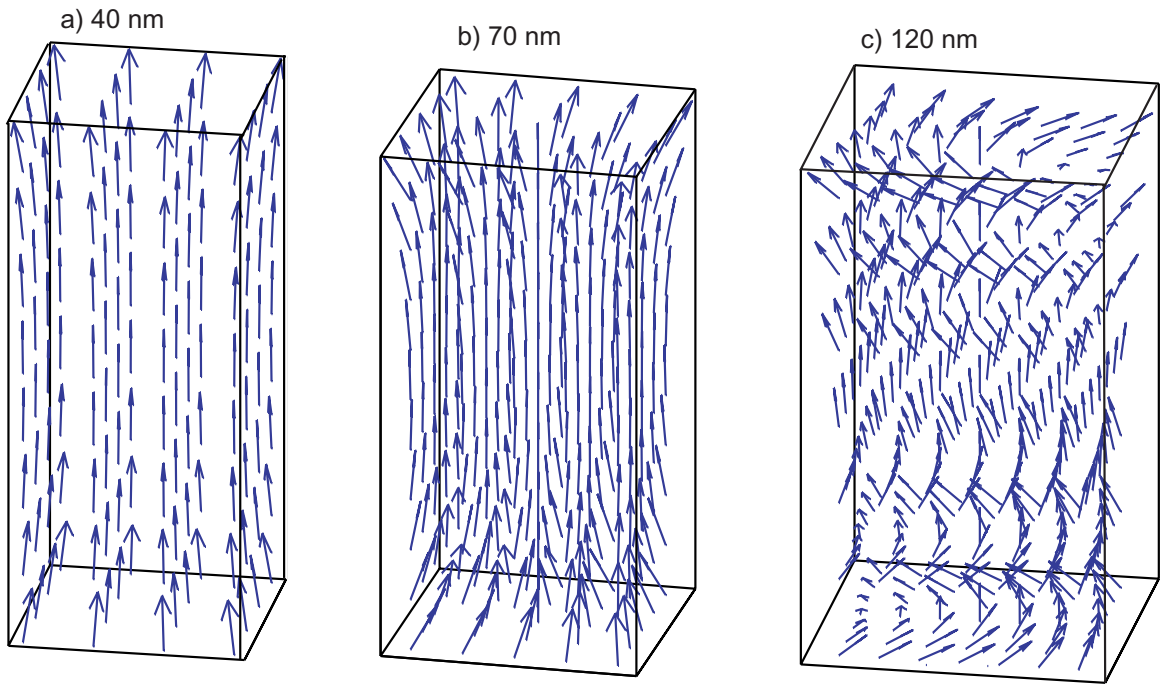

Figure 9. States of magnetizations for elongate particles (L/W = 2). (a) 40 nm particle exhibiting a weak flower state, (b) 70 nm particle, exhibiting a strong flower state, and (c) 120 nm particle exhibiting a double vortex state.

~100 nm, the "flowering" changes to a distinct remanent state whereby the tips of the particles are in a vortex state, while the central shaft is more or less uniformly magnetized along the particle length.

[53] In Figure 10a and 10b, we plot squareness and coercive field versus particle width respectively, for the uniaxial particle simulations. While squareness shows a monotonic decrease with particle width, there is a pronounced peak in coercive field, nearly twice the expected value of B_k or 57 mT. This peak is associated with the well developed flower states (as in Figure 9b). When the particle changes to the vortex state (e.g., Figure 9c) at around 100 nm, the coercive field decreases abruptly. These results echo those of *Schabes and Bertram* [1988] who found a comparable increase in coercive field of uniaxial particles with the field applied parallel to the easy axis for particles with flower remanent states.

5.4. More Complicated Shapes

[54] Photomicrographs of fine grained basalts suggest that neither cubes nor parallelepipeds are reasonable approximations for the shapes of the magnetic phases in these rocks [see, e.g., *Gee and Kent*, 1995]. These grains are referred to as "skeletal" (titano)magnetites. It is beyond the scope of this paper to model such grains in detail, but it is interesting to consider whether more complex shapes could yield hysteresis loops with coercive fields of the order of 100 mT, and squareness values higher than 0.5, as seen in some fine grained basalts (see Figure 4b).

[55] As an example of a more complicated particle shape, we model three intersecting parallelepipeds. In the example shown in Figure 11, each limb has three cells of 20 nm width for a total of 19 cells. We show the orientation of the remanent magnetization vectors after saturation in a field applied along the [111] direction. There is a net remanent magnetization of ~0.69 M_s in that direction. The magnetization is higher than would result if all the magnetization vectors were constrained to lie in the directions of the crystal limbs [0.57]. At the center of the particle, the magnetization vectors are deflected slightly toward the easy magnetocrystalline axis [111]. This simulated particle had a coercive field of 90 mT, far higher than that possible for magnetocrystalline dominated par-

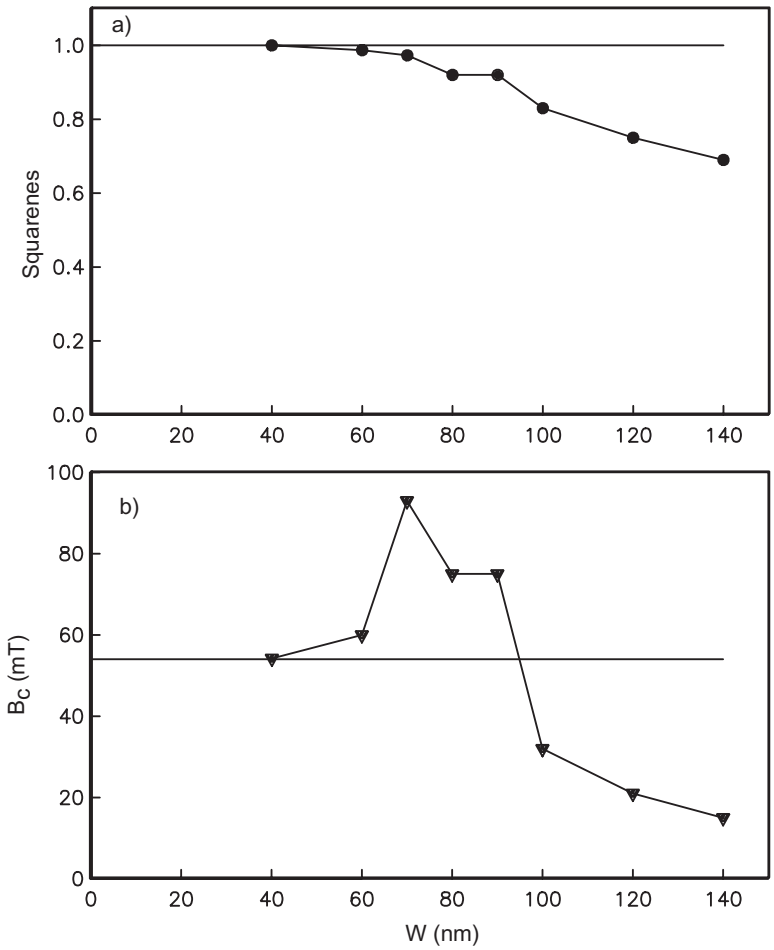

Figure 10. Hysteresis parameters versus particle width *W*. (a) Squareness. (b) Coercive field B_c.

ticles of magnetite, assuming the values for K_1 listed in Table 1.

[56] Larger intersecting rod particles were modeled by increasing the discretization along the limbs. In the section 5.5, simulations of particles with limbs having cross sections with 2 × 2 and 4 × 4 cell dimensions were performed with limb widths of 30 and 70 nm, respectively.

5.5. Assemblages of Uniformly Distributed Particles

[57] Hysteresis loops in paleomagnetism are measured on assemblages of particles that are usually uniformly distributed with respect to the applied field. We have simulated uniform distributions for single domain uniaxial and cubic particles in Figure 3a and 3b, respectively. Here we present results of full hysteresis loop simulations on various assemblages of particles.

[58] Examples of our simulations of uniformly distributed assemblages are shown in Figure 12. To simulate a uniform distribution, we chose a set of 12 directions spaced systematically over one-eighth of a sphere. We perform the simulations by setting the orientation (ϕ, θ in Figure 2c) between the applied field and the crystallographic axis and evaluating a full hysteresis loop. The results from each set of ϕ, θ are normalized by a solid angle ($\sin\theta d\theta d\phi$) to obtain the contribution of that orientation to the total hysteresis loop. In Figure 12a we show the results from equant particles with widths of ~90 nm. The thin lines are individual loops for a given ϕ, θ and the average loop is the heavy line in Figure 12a. The loop

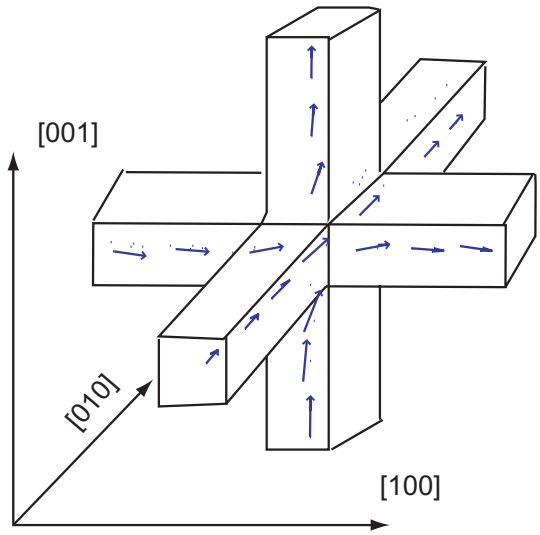

Figure 11. Results from a particle comprising three intersecting parallelepipeds. Each "limb" is composed of three cells. We take the cell width to be 20 nm in this simulation. Directions for the remanent magnetic vectors after saturation in the [111] direction. The net magnetization in that direction (squareness) is 0.69.

from a uniform assemblage of such particles has a squareness of 0.63 and a coercive field of 14 mT. As mentioned previously, the expected values (Table 1) are 0.87 and 10 mT for uniformly magnetized equant (CSD) particles of magnetite, respectively.

[59] In Figure 12b we show a similar set of curves for an assemblage of 70 nm particles with L/W ratios of 2. The average loop is shown as a heavy line in Figure 12a. The squareness of this assemblage is 0.46, and the coercive field is ~38 mT as compared to 0.5 and 69 mT (Table 1). These particles therefore have lower coercive fields than expected from a random assemblage, despite the enhanced coercive field of particles with favorable orientations to the applied field. This result underscores the difficulty of predicting the behavior of random assemblages from results of single field orientations.

[60] A third example of an assemblage of particles in shown in Figure 12c. This is for an assemblage of 115 nm equant particles. The average loop has a squareness of 0.16 and coercive field of 10 mT, typical of the "PSD" behavior often observed in rocks (see Figure 1a).

[61] We summarize the results of all our simulations of random arrays of particles in the squareness-coercive field plot shown in 13a. The squares are the results for equant particles. The triangle is a particle with a L/W ratio of 1.3. The rectangles are results from particles with L/W ratios of 2. The width of each particle is shown beside each point. The stars represent results from the assemblages of particles comprising intersecting rods. Several of the points in Figure 13a are derived from the simulations shown in Figures 3 and 12. The equant particles with widths of 90 and 115 nm have vortex remanent states. The 70 nm elongate particles had flower remanent states as did the 80 nm equant

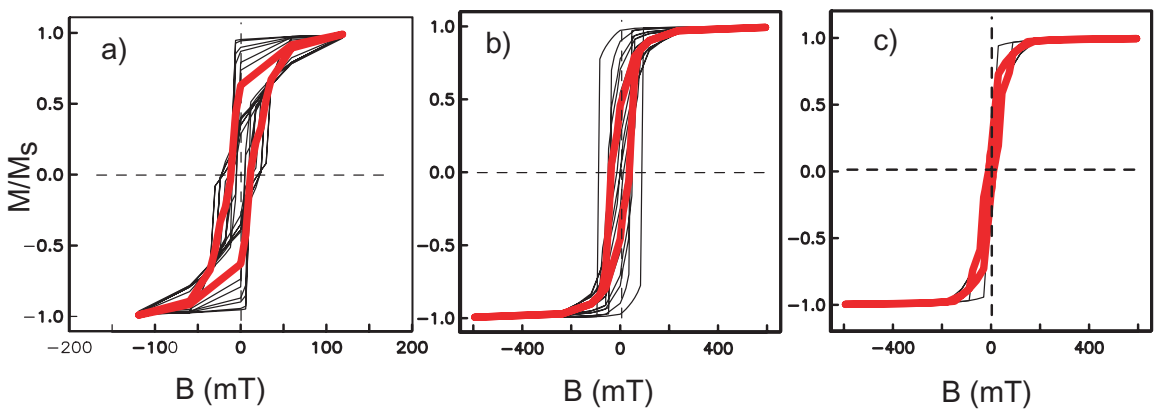

Figure 12. Simulated hysteresis loops for assemblages of randomly oriented particles. (a) Simulation of a 5 × 5 × 5 discretization scheme for a 90 nm particle. Thin lines are representative examples for various ϕ, θ). Heavy line is the average loop for a random assemblage of particles. (b) same as Figure 12a but for 5 × 5 × 10 discretization at 70 nm. (c) same as Figure 12a but for 7 × 7 × 7 discretization scheme at 115 nm.

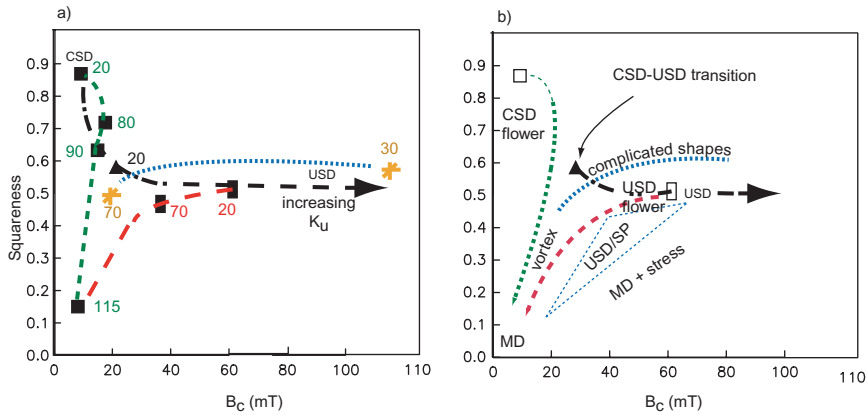

Figure 13. Squareness versus coercive field plots. (a) Summary of the simulations of hysteresis loops for randomly oriented particles of different sizes and shapes. Squares are equant particles. The triangle is for a particle with aspect ratio of 1.3:1. The rectangles are for particles with aspect ratios of 2:1. The stars are for three intersecting rods. The particle widths (nm) are shown next to the particles. CSD is cubic single domain. USD is uniaxial single domain. Uniformly magnetized particles with increasing aspect ratios will plot along the heavy dashed-dot line joining the USD line at aspect ratio of approximately 1.5:1. Increasing particle sizes will plot along the dashed lines toward the origin. (b) Interpretations of the data discussed in this paper (see text).

particles. The tips of the rods in the intersecting rods particles were in the vortex remanent state for the 70 nm particle and were more flower-like in the 40 nm particle.

6. Discussion

6.1. Interpretation of Results

[62] In Figure 13b, we sketch our interpretations of the results discussed in this paper for squareness-coercive field behavior for various sizes and shapes. According to *Butler and Banerjee* [1975] equant particles of magnetite do not exist in the single domain state. If this is true, there can be no mixing of superparamagnetic and CSD behaviors. As particle width increases, however, perhaps with the onset of the flower state, coercive field increases and the behavior of such particles is predicted to lie along the trend labeled "CSD flower". Both coercive field and squareness decrease with increasing size (>∼80 nm) as the flower structure fades and the curling reversal mode associated with the vortex remanent state begins to dominate.

[63] Uniformly magnetized particles with increasing aspect ratios move from the CSD field to uniaxial behavior along the dash-dot line in Figure 13a. According to *Butler and Banerjee* [1975], most of this trend will be in the superparamagnetic region until perhaps a length to width ratio of about 1.3:1 (shown as a triangle). We have drawn the CSD-USD transition line as a dash dot trending from the 20 nm 1.3:1 result to the 2:1 USD result in Figure 13b.

[64] Particles reversing by uniform rotation and aspect ratios larger than 1.5:1 will have a squareness of 0.5 and coercive fields increasing to a maximum of about 300 mT (see Table 1) or larger if stress plays a role. As particle width for these essentially uniaxial particles increases, the coercive field decreases, while maintaining relatively high squareness values until the vortex state is established. The ability to reverse by curling drives both the coercive field and squareness toward the MD region (near the origin). Finally, assemblages of more complex particles (the intersecting rods in Figure 13a) can have coercive fields comparable to USD magnetites yet have squarenesses higher than the 0.5 expected from USD. We have sketched a curve labeled "complicated shapes" to reflect the results of these simulations.

6.2. Application to Published Data

[65] The vast majority of hysteresis data from geological materials plot in the "PSD" box of the Day diagram. We see from Figure 13b that

there are in fact at least three types of behavior that control hysteresis in this realm: (1) mixing of USD and SP behaviors causing a depression of squareness and coercive fields but along a mixing line connecting the origin and the USD points, (2) onset of curling reversal mode causing a depression of squareness and coercive field, and (3) stress in essentially multidomain particles which enhances the uniaxial anisotropy constant and suppresses domain wall nucleation and motion thus allowing higher squareness and coercive field values than in unstressed particles of comparable size. It is also worth mentioning that mixtures of two phases (e.g., magnetite and hematite) will also place a given sample in the PSD box (see, e.g., *Tauxe et al.* [1996] for techniques to distinguish this from USD/SP mixing).

[66] On the basis of our interpretation of the simulations discussed here, we suggest that the hysteresis behavior plotted as open triangles in Figure 4b (see figure caption for sources) is controlled by mixing USD and superparamagnetic particles. This contention is supported by the data of *Schmidbauer and Schembera* [1987] who made measurements of similar samples at low temperature in order to suppress the contribution of superparamagnetism. Their data (squares in Figure 4b) plot parallel to the "CSD-flower" trend but with slightly higher coercive fields. The offset could be the result of the fact that the particles were slightly elongate.

[67] The solid triangle in Figure 4b represents the hysteresis behavior of magnetite particles obtained from magnetotactic bacteria [*Moskowitz et al.*, 1988]. These particles are very uniform in size and have average particle dimensions of ~45 nm [*Dunin-Borkowski et al.*, 1998]. The data exhibit the squareness values that are essentially those predicted by a uniaxial model, while the particles are cubic in shape. Presumably, the fact that they are arrayed in long chains explains the uniaxial behavior.

[68] The data presented by *Gee and Kent* [1995] for fine grained oceanic basalts was also shown in Figure 4b. It is difficult to explain such hysteresis data with coercive fields higher than those expected for USD magnetite with $L/W >$ 1.5 and squareness values higher than 0.5 with either elongate or equant particles. It is also difficult to call on USD-CSD transitional particles because the trend is orthogonal to that expected and many samples have much too large coercive fields. As mentioned previously, photomicrographs of samples exhibiting such high squareness-coercive field behavior [see, e.g., *Gee and Kent*, 1995] show skeletal particles whose shapes are certainly not well approximated as a parallelepiped. In order to address the issue of whether high squareness-very high coercive field (>60 mT) behavior could result from more complex shapes, we "built" a particle that was a three-dimensional cross, elongate along the three axes sketched in Figure 11a. The squareness and coercive field of several simulations are marked with 3-D cross symbol (stars) in Figure 13a and are labeled as to limb width in nanometers. As the particles become larger, the magnetization structures become more complicated lowering coercive field and ultimately squareness as indicated by the simulations for a 70 nm intersecting rod particle. From this simple approximation, it appears likely that the trend observed in the fine grained oceanic basalts of *Gee and Kent* [1995, 1999] could be caused by shapes more complex than simple rods or cubes.

[69] Rock samples with squareness values between 0.5 and 0.05 are routinely interpreted in the environmental magnetism literature as being "PSD" and are ascribed to grain size range of 1–15 μm. The interpretation as to grain size stems from a set of hysteresis data for crushed (titano) magnetites compiled by *Day et al.* [1977] (squares on Figure 4b). It has long been known that the data from crushed particles for a given grain size range are quite different than uncrushed particles of the same size [e.g., *Dunlop*, 1986]. On the traditional Day diagram, the data for uncrushed magnetites in the size range of up to ~100 nm (shown as open triangles on Figure 4b) plot on top of the data for 1–15 μm crushed magnetites (shown as squares). These two data sets plot in an entirely different regions in the squareness-coercive field plot used here. We were completely unable to obtain PSD-like values of squareness (0.05–0.5) for particles

larger than ~140 nm and agree with the contention that the crushed particles have sources of anisotropy other than shape or magnetocrystalline. We suppose that domain wall nucleation is suppressed by the presence of dislocations, enhancing squareness and that these walls are pinned to some extent, enhancing coercive field (see *Dunlop and Özdemir* [1997] for an insightful discussion). In any case, it appears that stress dominated particles (with larger grain sizes) can be distinguished from unstressed particles (with much smaller grain sizes) using a squareness-coercive field diagram shown in Figure 13b rather than the "Day diagram."

7. Conclusions

1. We have confirmed the existence of the "flower" remanent magnetization state in uniaxial particles in the size of 70–80 nm [e.g., *Schabes and Bertram*, 1988] and that the flower state has a higher coercive field than the strictly uniformly magnetized state in which all the spins are essentially parallel.

2. Assemblages of equant grains in the flower state can have squarenesses above the uniaxial expectation of 0.5 and coercive fields above the cubic expectation for magnetite and TM60 of 10 mT. Nonetheless, the maximum coercive field for assemblages of equant grains that we observed was ~20 mT, far less than the ~100 mT observed in some fine grained oceanic basalts.

3. Inequant particles with aspect ratios less than 1.5:1 have properties transitional between uniaxial and strictly cubic particles with intermediate squareness and coercive field.

4. We have confirmed the role of "vortex" remanent states in contributing to "pseudosingle domain" hysteresis behavior as suggested by *Williams and Dunlop* [1995].

5. Particles with more complex shapes than simple rods and cubes, such as three intersecting and mutually orthogonal parallelepipeds, provide a plausible explanation for the very high coercive field, high squareness values observed in some fine grained oceanic basalts.

6. It is clear that the possibility for unambiguous interpretation of hysteresis in terms of grain size and shape remains remote. The same remanence and coercive field is exhibited by assemblages of particles of quite different grain size and shape. However, more micromagnetic modeling of particles with different types of mineralogies, sizes, and shapes can provide further constraints. In addition, modeling of assemblages with distributions of properties and the inclusion of finite temperature would be helpful.

Acknowledgments

[70] We are indebted to Daniel Staudigel who generated the movies used to illustrate magnetic reversal behavior. We would like to thank Jeff Gee for many helpful discussions and comments on the manuscripts. Thanks go to Peng Luo and Kurt Schwehr for help in the early phases of the work. We also thank Julie Bowles for critically reading the manuscript. This work benefitted from conversations with Wyn Williams, Karl Fabian, and David Dunlop and from two anonymous reviews as well as the comments of Dennis Kent and Bruce Moskowitz. This work was partially supported by NSF grant 9814390 to LT.

References

Bertram, H. N., and J.-G. Zhu (Eds.), *Fundamental Magnetization Processes in Thin-Film Recording Media*, *Solid State Physis*, vol. 46, Academic, San Diego, Calif., 1992.

Brown, W., *Micromagnetics*, Wiley-Interscience, New York, 1963.

Butler, R. F., and S. K. Banerjee, Theoretical single domain grain-size range in magnetite and titanomagnetite, *J. Geophys. Res.*, *80*, 4049–4058, 1975.

Day, R., M. D. Fuller, and V. A. Schmidt, Hysteresis properties of titanomagnetites: Grain size and composition dependence, *Phys. Earth Planet. Inter.*, *13*, 260–266, 1977.

Dunin-Borkowski, R. E., M. R. McCartney, R. B. Frankel, D. A. Bazylinski, M. Posfai, and P. R. Buseck, Magnetic microstructure of magnetotactic bacteria by electron holography, *Science*, *282*, 1868–1870, 1998.

Dunlop, D., Thermoremanent magnetization in submicroscopic magnetite, *J. Geophys. Res.*, *78*, 7602–7613, 1973.

Dunlop, D. J., Hysteresis properties of magnetite and their dependence on particle size: A test of PSD remanence models, *J. Geophys. Res.*, *91*, 9569–9584, 1986.

Dunlop, D., and O. Özdemir, *Rock Magnetism: Fundamentals and Frontiers*, *Cambridge Studies in Magnetism Ser.*, vol. 3, Cambridge Univ. Press, New York, 1997.

Fabian, K., and A. Hubert, Shape-induced pseudo-single-domain remanence, *Geophys. J. Int.*, *138*, 717–726, 1999.

Fabian, K., and T. von Dobeneck, Isothermal magnetization of samples with stable Preisach function: A survey of hysteresis, remanence and rock magnetic parameters, *J. Geophys. Res.*, *102*, 17,659–17,677, 1997.

Fabian, K., K. Andreas, W. Williams, F. Heider, T. Leibl, and A. Huber, Three-dimensional micromagnetic calculations for magnetite using FFT, *Geophys. J. Int.*, *124*, 89–104, 1996.

Flanders, P. J., An alternating gradient force magnetometer, *J. Appl. Phys.*, *63*, 3940–3945, 1988.

Frei, E., S. Shtrikman, and D. Treves, Critical size and nucleation field of ideal ferromagnetic particles, *Phys. Rev.*, *106*, 446–455, 1957.

Gee, J. S., and D. V. Kent, Magnetic hysteresis in young mid-ocean ridge basalts: Dominant cubic anisotropy?, *Geophys. Res. Lett.*, *22*, 551–554, 1995.

Gottschalk, V., The coercive force of magnetite powders, *Physics*, *6*, 127–132, 1935.

Halgedahl, S., and M. Fuller, The dependence of magnetic domain structure upon magnetization state with emphasis upon nucleation as a mechanism for pseudo-single domain behavior, *J. Geophys. Res.*, *88*, 6505–6522, 1983.

Heider, F., and W. Williams, Note on temperature dependence of exchange constant in magnetite, *Geophys. Res. Lett.*, *15*, 184–187, 1988.

Heider, F., D. J. Dunlop, and N. Sugiura, Magnetic properties of hydrothermally resrystallized magnetite crystals, *Science*, *236*, 1287–1290, 1987.

Joffe, I., and R. Heuberger, Hysteresis properties of distributions of cubic single-domain ferromagnetic particles, *Philos. Mag.*, *314*, 1051–1059, 1974.

Kent, D. V., and J. Gee, Magnetic alteration of zero-age oceanic basalt, *Geology*, *24*, 703–706, 1996.

Moskowitz, B. M., R. B. Frankel, P. J. Flanders, R. P. Blakemore, and B. B. Schwartz, Magnetic properties of magnetotactic bacteria, *J. Magn. Magn. Mater.*, *73*, 273–288, 1988.

Muxworthy, A., and W. Williams, Micromagnetic models of pseudo-single domain grains of magnetite near the Verwey transition, *J. Geophys. Res.*, *104*, 29,203–29,217, 1999a.

Muxworthy, A., and W. Williams, Micromagnetic calculation of hysteresis as a function of temperature in pseudo-single domain magnetite, *Geophys. Res. Lett.*, *26*, 1065–1068, 1999b.

Nagata, T., *Rock Magnetism*, Maruzen, Tokyo, 1953.

Newell, A., and R. Merrill, Nucleation and stability of ferromagnetic states, *J. Geophys. Res.*, *105*, 19,377–19,391, 2000a.

Newell, A., and R. Merrill, Size dependence of hysteresis properties of small pseudo-single-domain grains, *J. Geophys. Res.*, *105*, 19,393–19,403, 2000b.

Parry, L., Magnetic prperties of dispersed magnetite powders, *Philos. Mag.*, *11*, 303–312, 1965.

Pick, T., and L. Tauxe, Characteristics of magnetite in submarine basaltic glass, *Geophys. J.*, *119*, 116–128, 1994.

Rave, W., K. Fabian, and A. Hubert, Magnetic states of small cubic particles with uniaxial anisotropy, *J. Magn. Magn. Mater.*, *190*, 332–348, 1998.

Schabes, M. E., and H. N. Bertram, Magnetization processes in ferromagnetic cubes, *J. Appl. Phys.*, *64*, 1347–1357, 1988.

Schmidbauer, E., and N. Schembera, Magnetic hysteresis properties and anhysteretic remanent magnetization of spherical Fe_3O_4 particles in the grain range 60–160 nm, *Phys. Earth Planet. Int.*, *46*, 77–83, 1987.

Seberino, C., Computational micromagnetic study of particulate media: Hysteresis and recording, Ph.D. thesis, Univ. of Calif., San Diego, 2000.

Seberino, C., and H. N. Bertram, Concise, efficient three-dimensional fast multipole method for micromagnetics, *IEEE Trans. Magn.*, *37*, 1078–1086, 2001.

Shive, P., Dislocation control of magnetization, *J. Geomag. Geoelectr.*, *21*, 519–529, 1969.

Smit, J., and H. Wijn, *Ferrites: Physical Properties of Ferrimagnetic Oxides in Relation to Their Technical Applications*, pp. 1–157, John Wiley, New York, 1959.

Stacey, F., Theory of the magnetic properties of igneous rocks in alternating fields, *Philos. Mag.*, *6*, 1241–1260, 1961.

Stacey, F., A generalized theory of thermoremanence, covering the transition from single domain to multi-domain magnetic grains, *Philos. Mag.*, *7*, 1887–1900, 1962.

Stacey, F. D., The physical theory of rock magnetism, *Adv. Phys.*, *12*, 45–133, 1963.

Stacey, F. D., and S. K. Banerjee, *The Physical Principles of Rock Magnetism*, vol. 5 *Developments in Solid Earth Geophysics*, Elsevier Sci., New York, 1974.

Stoner, E. C., and W. Wohlfarth, A mechanism of magnetic hysteresis in heterogeneous alloys, *Philos. Trans. R. Soc. London*, *A240*, 599–642, 1948.

Tauxe, L., T. A. T. Mullender, and T. Pick, Potbellies, wasp-waists, and superparamagnetism in magnetic hysteresis, *J. Geophys. Res.*, *101*, 571–583, 1996.

Verhoogen, J., The origin of thermoremanent magnetization, *J. Geophys. Res.*, *64*, 2441–2449, 1959.

Walker, M., P. I. Mayo, K. O. Grady, S. W. Charles, and R. W. Chantrell, The magnetic properies of single-domain particles with cubic anisotropy: 1 hysteresis loops, *J. Phys. Condens. Matter*, *5*, 2779–2792, 1993.

Williams, W., and D. J. Dunlop, Three-dimensional micromagnetic modelling of ferromagnetic domain structure, *Nature*, *337*, 634–637, 1989.

Williams, W., and D. Dunlop, Simulation of magnetic hysteresis in pseudo-single-domain grains of magnetite, *J. Geophys. Res.*, *100*, 3859–3871, 1995.

Williams, W., and T. Wright, High-resolution micromagnetic models of fine grains of magnetite, *J. Geophys. Res.*, *103*, 30,537–30,550, 1998.

Wohlfarth, E. P., Relations between different modes of acquisition of the remanent magnetisation of ferromagnetic particles, *J. Appl. Phys.*, *29*, 595–596, 1958.

Yang, B., and D. R. Fredkin, Dynamical micromagnetics of a ferromagnetic particle: Numerical studies, *J. Appl. Phys.*, *79*, 5755–5757, 1996.